Chemical Science

ROYAL SOCIETY OF CHEMISTRY

EDGE ARTICLE

View Article Online
View Journal | View Issue

Cite this: *Chem. Sci.*, 2024, **15**, 964

All publication charges for this article have been paid for by the Royal Society of Chemistry

Received 30th August 2023
Accepted 1st December 2023

DOI: 10.1039/d3sc04564a

rsc.li/chemical-science

Enhanced solid-state phosphorescence of organoplatinum π-systems by ion-pairing assembly†

Yohei Haketa,[a] Kaifu Komatsu,[a] Hiroi Sei,[b] Hiroki Imoba,[b] Wataru Ota,[c] Tohru Sato,[de] Yu Murakami,[a] Hiroki Tanaka,[a] Nobuhiro Yasuda,[f] Norimitsu Tohnai[b] and Hiromitsu Maeda *[a]

Anion binding and ion pairing of dipyrrolyldiketone Pt^{II} complexes as anion-responsive π-electronic molecules resulted in photophysical modulations, as observed in solid-state phosphorescence properties. Modifications to arylpyridine ligands in the Pt^{II} complexes significantly impacted the assembling behaviour and photophysical properties of anion-free and anion-binding (ion-pairing) forms. The Pt^{II} complexes, in the presence of guest anions and their countercations, formed various anion-binding modes and ion-pairing assembled structures depending on constituents and forms (solutions and crystals). The Pt^{II} complexes emitted strong phosphorescence in deoxygenated solutions but showed extremely weak phosphorescence in the solid state owing to self-association. In contrast, the solid-state ion-pairing assemblies with tetraalkylammonium cations exhibited enhanced phosphorescence owing to the formation of hydrogen-bonding 1D-chain Pt^{II} complexes dispersed by stacking with aliphatic cations. Theoretical studies revealed that the enhanced phosphorescence in the solid-state ion-pairing assembly was attributed to preventing the delocalisation of the electron wavefunction over Pt^{II} complexes.

Introduction

π-Electronic molecules in ordered arrangements demonstrate fascinating electronic and electrooptical properties that are not observed in single molecules.[1] Introducing multiple building units in assemblies induces properties that can be modulated by constituent species. Among organic materials, solid-state luminescent materials have received significant attention owing to their applications in light-emitting diodes, sensors and photonics.[2] In particular, crystals of square-planar organoplatinum(II) complexes exhibit fascinating photoluminescence properties,[3,4] such as triplet energy transfer and phosphorescence anisotropy amplification.[4h,j] The solid-state luminescence of π-electronic species is frequently quenched or weakened by self-association (Fig. 1a left), primarily because

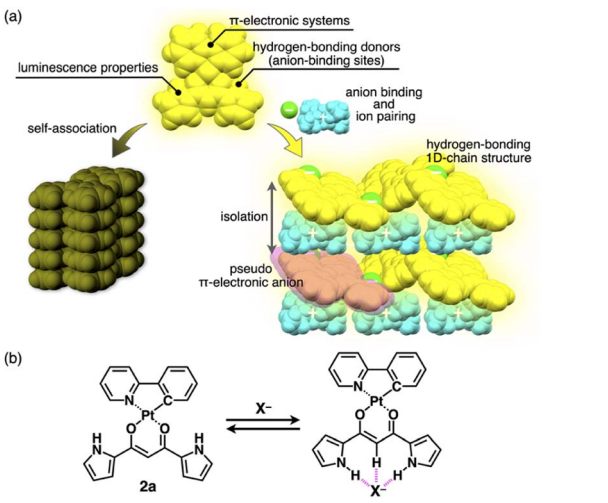

Fig. 1 (a) Conceptual diagram of anion binding and ion pairing for emission enhancement: stacking structure of anion-responsive luminescent molecules (left) and charge-by-charge assembly with hydrogen-bonding 1D-chain structures of receptor–anion complexes as pseudo π-electronic anions (right) and (b) anion complexation of dipyrrolyldiketone Pt^{II} complex **2a**.

[a]*Department of Applied Chemistry, College of Life Sciences, Ritsumeikan University, Kusatsu 525-8577, Japan. E-mail: maedahir@ph.ritsumei.ac.jp*

[b]*Department of Applied Chemistry, Graduate School of Engineering, Osaka University, Suita 565-0871, Japan*

[c]*MOLFEX, Inc., Kyoto 606-8103, Japan*

[d]*Fukui Institute for Fundamental Chemistry, Kyoto University, Kyoto 606-8103, Japan*

[e]*Department of Molecular Engineering, Graduate School of Engineering, Kyoto University, Kyoto 615-8510, Japan*

[f]*Beamline Division, Japan Synchrotron Radiation Research Institute, Sayo 679-5198, Japan*

† Electronic supplementary information (ESI) available: Synthetic procedures, analytical data, computational details and CIF files for the single-crystal X-ray structural analysis. CCDC 2158662–2158674. For ESI and crystallographic data in CIF or other electronic format see DOI: https://doi.org/10.1039/d3sc04564a

of exciton coupling between neighbouring molecules.[5,6] To prevent this, introducing bulky groups to interfere with the molecular contact is an effective strategy for enhancing solid-state luminescence by electronic decoupling of organoplatinum π-systems.[4c,e,j,7] Therefore, appropriate isolation arrangements for emissive species have been highly demanded. Furthermore, it is important to maintain rigid structures to decrease the rates of non-radiative decay processes that interfere with phosphorescent emission.[3c,8] Thus, both isolation and robustness in packing structures are required for effective luminescence.

Ion pairs, which comprise complementarily associated positively and negatively charged species, can be employed for an isolation strategy.[9,10] Isolation and electronic decoupling of luminescent cations have been achieved by introducing bulky counteranions.[11] Furthermore, ion complexation by ion-responsive π-electronic molecules (receptors) followed by pairing with counterions is appropriate for preparing π-electronic ion pairs. This method can be used to create pseudo-π-electronic anions in the form of receptor–anion complexes. Spatially and electronically isolated charged fluorophores (cationic dyes) exhibit fluorescence emission in the solid state when combined with well-designed counter species (anion complexes).[12] In contrast, including photo-functional anion-responsive π-electronic systems would also provide luminescent crystalline states through anion complexation with hydrogen bonding and alternate stacking with countercations (Fig. 1a right). The anion complexation would give rise to rigid structures by hydrogen bonds tightly connecting building units (pseudo-π-electronic anions comprising luminescent receptors) with the support of the charge-by-charge arrangement by electrostatic and dispersion forces. Designing luminescent anion receptors and combining them with countercations for isolation enable the control of the photophysical properties.

As luminescent π-electronic systems, dipyrrolyldiketone Pt^{II} complexes (*e.g.*, **2a**, Fig. 1b), with phenylpyridine (ppy) as a C^N ligand, have been synthesized as phosphorescent anion sensors, exhibiting absorption and emission maxima (λ_{max} and λ_{em}, respectively) at 410 and 510 nm, respectively, with an emission quantum yield (Φ_{em}) of 42% for **2a** in CH_2Cl_2.[13] Planar geometries around Pt^{II} with a ppy ligand are suitable for stacking structures by themselves and in the form of ion-pairing assemblies.[14] The Pt^{II} complexes would exhibit luminescent properties according to the introduced C^N ligands in solution and ion-pairing assemblies. Furthermore, the solid-state luminescent properties, whose control by countercations is also challenging, have not been elucidated. In this study, enhanced solid-state phosphorescence was achieved by ion pairing and the isolation of emissive anion complex moieties by countercations, for diverse Pt^{II} complexes.

Results and discussion

Synthesis and characterization of Pt^{II} complexes

Four different C^N ligands were used to produce Pt^{II} complexes **2b–e** in 7.0–27% yields by treating dipyrrolyldiketone **1** with the mixture of the ligands and $[(PtMe_2)_2(SMe_2)_2]$[15] at r.t. in the presence of trifluoromethanesulfonic acid (TfOH) (1 equiv.) and K_2CO_3 (1.5 equiv.) (Fig. 2). The obtained Pt^{II} complexes were characterized by ^1H and ^{13}C NMR and ESI-TOF-MS. Conformations without pyrrole inversions (*py0i* conformations) were suggested by the theoretically optimized structures: doubly pyrrole-inverted (*py2i*) conformations of **2b–e**, suitable for anion binding, were less stable by 6.84, 6.79, 7.10 and 6.15 kcal mol^{-1}, respectively, due to the enhanced molecular electric dipoles.[16]

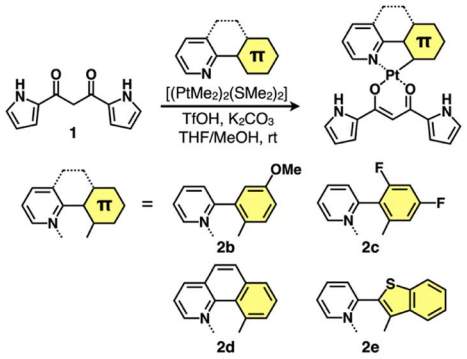

Fig. 2 Synthesis of dipyrrolyldiketone Pt^{II} complexes **2b–e**.

Solution-state properties

The UV/vis absorption spectra of **2b–e** in CH_2Cl_2 exhibited the λ_{max} at ~310–450 nm, and the spectral features, λ_{max} values and absorbance intensities, were complicated depending on the introduced ligand moieties (Fig. 3 and Table 1). For example, **2b** displayed the λ_{max} at 368, 390 and 412 nm, and similar spectral features were observed in **2c,d**, whereas **2e** exhibited a distinctive spectrum with the λ_{max} at 388 and 409 nm along with those at 318 and 455 nm. Similarly to **2a**,[13] the main absorption bands of **2b–e** were assigned as the lowest-lying singlet states, originating primarily from the HOMO-to-LUMO transition with a significant contribution from ligand-to-ligand charge transfer (LLCT) from the dipyrrolyldiketone unit to the arylpyridine ligands and metal-to-ligand charge transfer (MLCT) from Pt^{II} to

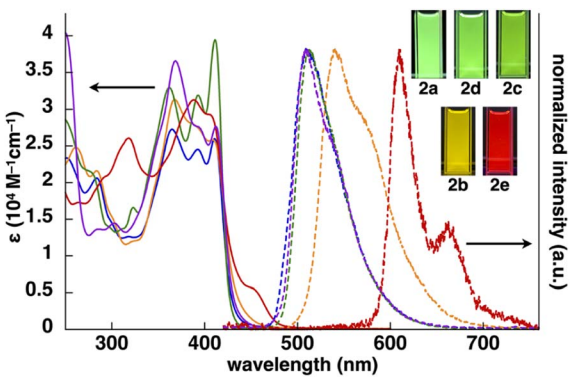

Fig. 3 UV/vis absorption spectra (solid lines, CH_2Cl_2) and normalized emission spectra (dashed lines, deoxygenated CH_2Cl_2) with the excitation at 410, 368, 411, 368 and 388 nm of **2a** (blue), **2b** (orange), **2c** (green), **2d** (purple) and **2e** (red) (inset: photographs of Pt^{II} complexes under UV_{365} (0.03 mM)).

Table 1 Summary of the UV/vis absorption (λ_{max}) and emission (λ_{em}) maxima with quantum yields (Φ_{em}) of **2b–e** with **2a** [a] as a reference in CH_2Cl_2

	λ_{max} [b] [nm]	λ_{em} [nm]	Φ_{em} [%]	τ [μs]
2b	**368**/390/412	542	68	4.6
2c	361/393/**411**	512	50	9.6
2d	**368**/390/408	508	50	4.2
2e	**388**/409	610/662(sh)	16	6.8
2a [a]	364/393/**410**	510	42	5.1

[a] Ref. 13. [b] Excitation wavelengths for emission spectra are in bold.

arylpyridine ligands; the theoretical study was conducted using time-dependent (TD)-DFT calculations at the CAM-B3LYP level using the 6-31+G(d,p) basis set with the LanL2DZ basis set and associated effective core potentials for Pt, which were used for the calculations in the following parts.[16] Furthermore, characteristic absorption bands of **2e** at 318 and 455 nm can be attributed to the π–π* transition of the benzothienyl-pyridine ligand and intraligand charge transfer from the π orbitals of the benzo unit to the π* orbitals of the pyridyl group, respectively.[17]

The phosphorescence spectra of **2b–e** in deoxygenated CH_2Cl_2 exhibited broad emission bands with a λ_{em} of 542, 512, 508 and 610/662(sh) nm, respectively (Fig. 3 and Table 1), suggesting the red-shifted emissions for **2b,e** compared to **2a**. The Φ_{em} of **2b–d** were 68%, 50% and 50%, respectively, which were greater than that of **2e** (16%). The phosphorescence emissions of **2b–e** originating from the triplet states were suggested by the emission lifetimes (τ) of 4.6, 9.6, 4.2 and 6.8 μs, respectively, similar to that of **2a** (5.1 μs).[13] TD-DFT calculations for the optimized T_1 structures at the PCM-M06-2X level in CH_2Cl_2 showed theoretically estimated emission maxima at 499, 524, 495 and 714 nm for **2b–e**, respectively, which are close to the observed values (Fig. S56†). The phosphorescence emissions of **2c,e** were mainly derived from the LUMO-to-HOMO (84% and 96%, respectively) transitions, whereas those of **2b,d** were ascribed to the LUMO-to-HOMO−1 (68%) and LUMO+1-to-HOMO (60%) transitions, respectively.

Anion-binding behaviours were revealed by ^{1}H NMR spectral changes in CD_2Cl_2 (1.0 mM) (Fig. S74–S77†). Upon the addition of 3.3 equiv. of tetrabutylammonium chloride (TBACl) to, as an example, **2c**, the signals of the pyrrole NH and bridging CH at 9.35/9.31 and 6.41 ppm, respectively, at −50 °C disappeared, whereas the corresponding new signals appeared at 12.55/12.49 and 7.42 ppm, respectively. The downfield shifts were caused by hydrogen bonding with Cl^-, implying the formation of [1 + 1]-type Cl^- complexes, as demonstrated by theoretical studies (Fig. S39–S42†).[16]

The anion-binding constants (K_a) of **2b–e** in a [1 + 1]-binding mode were evaluated by the changes in UV/vis absorption spectra caused by the addition of anions (Cl^-, Br^- and $CH_3CO_2^-$) as TBA salts in CH_2Cl_2 (Table 2 and Fig. S70–S73†). In all the derivatives discussed in this study, the K_a values were in the order of $CH_3CO_2^- > Cl^- > Br^-$ correlating with the basicity. Cl^- complexation produced phosphorescence emissions (λ_{em} at 542, 505, 511 and 610/660 nm for **2b–e**, respectively) with Φ_{em} (54%, 32%, 41% and 14%, respectively) and τ (4.3–14.2 μs), which were comparable to those of **2a**·Cl^- (λ_{em}: 490/520 nm, Φ_{em}: 48%, τ: 2.4 μs) (Table 3). It should be noted that anion complexation of the Pt^{II} complexes in solution did not significantly affect the emission properties. Pt^{II} complexes with such emission properties can be used as building blocks for solid-state materials whose packing structures and resulting luminescent properties are modulated by anion complexation and ion pairing with countercations.

Table 2 Anion-binding constants (K_a, M^{-1}) of **2b–e** with **2a** [a] as a reference in CH_2Cl_2

	2b	**2c**	**2d**	**2e**	**2a** [a]
Cl^-	2000	2200	1200	1900	1300
Br^-	320	240	50	310	61
$CH_3CO_2^-$	7400	22 000	5400	15 000	15 000

[a] Ref. 13.

Table 3 Summary of the UV/vis absorption (λ_{max}) and emission (λ_{em}) maxima with quantum yields (Φ_{em}) of **2b–e** with **2a** [a] as a reference upon the addition of TBACl (2000 equiv. for **2b–e** and 3000 equiv. for **2d**) in CH_2Cl_2

	λ_{max} [b] [nm]	λ_{em} [nm]	Φ_{em} [%]	τ [μs]
2b	**372**/387/410	542	54	4.3
2c	367/390/**409**	505	32	6.4
2d	**372**/411	511	41	14.2
2e	**388**/409	610/660(sh)	14	6.8
2a [a]	369/389/**410**	490/520(sh)	48	2.4

[a] Ref. 13. [b] Excitation wavelengths for emission spectra with bold.

Solid-state luminescence and packing structures

In contrast to the phosphorescence emission in the dispersed solution state, the solid-state Pt^{II} complexes obtained from the single crystals (*vide infra*) exhibited extremely weak luminescence: **2a–e** exhibited λ_{em} at 523/682, 591, 673, 652 and 627 nm with Φ_{em} of 0.7%, ∼0.1%, 1.8%, ∼0.1% and ∼0.2%, respectively (Fig. S86–S90†).[18] Such red-shifted emission with emission quenching can be caused by the excimer formation of excited Pt^{II} complexes,[19] as theoretically discussed in the following section. Notably, the Φ_{em} of solid-state **2a–e** are lower than those of 1,3-diphenyl-1,3-propanedione Pt^{II} complexes.[4h] The details of the assembled structures were revealed by X-ray analysis for the single crystals of **2b–e** obtained by vapour diffusion of *n*-hexane into CH_2Cl_2 solutions (Fig. 4 and S19–S23†).[20] **2b–e** exhibited planar pyrrole-non-inverted (*py0i*) conformations in stacking structures, similar to **2a**,[13] with mean-plane deviations (defined by the core atoms without hydrogen atoms) of 0.103–0.174 Å. The Pt^{II} complexes **2b–e** formed columnar π–π stacking structures with stacking distances of 3.21–3.38 Å. Among them, **2b,e** showed stacked-dimer alignment with Pt⋯Pt distances of 3.46 and 3.29 Å,

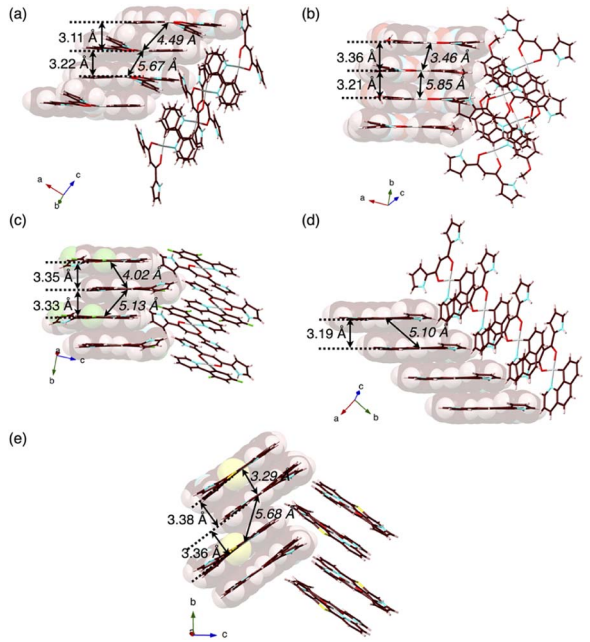

Fig. 4 Single-crystal X-ray structures, with selected stacking and Pt⋯Pt (italic) distances, of (a) **2a** as a reference,[13] and (b) **2b**, (c) **2c**, (d) **2d** and (e) **2e** as packing diagrams. Atom colour codes in Fig. 4 and the following figures: brown, pink, blue, red, yellow green, yellow and grey refer to carbon, hydrogen, nitrogen, oxygen, fluorine, sulfur and platinum, respectively.

respectively. The π–π stacking structures were identified by Hirshfeld surface analysis (Fig. S33–S37†).[20] There are no notable intermolecular interactions on the lateral side of the columnar π–π stacking structures except for **2c**, which showed N–H⋯π interactions between pyrrole rings.

The extremely weak crystal-state emissive properties were modulated by isolating the Pt^{II} complexes without stacking by themselves. Single crystals of the ion pairs **2a**·Cl^--TBA^+ and **2a**·Cl^--$TPeA^+$ ($TPeA^+$: tetrapentylammonium) were prepared by vapour diffusion of *n*-hexane into the THF solutions of **2a** and corresponding tetraalkylammonium salts (Fig. 5). The ion pair **2a**·Cl^--TPA^+ (TPA^+: tetrapropylammonium) was also prepared as precipitates by adding *n*-hexane to a mixture of **2a** and TPACl in CH_2Cl_2.[21] Compositions of the Cl^--binding Pt^{II} complex and countercations in all the solid-state samples were fully characterized by using ^1H NMR. In contrast to the anion-free states, solid-state **2a**·Cl^--TPA^+, **2a**·Cl^--TBA^+ and **2a**·Cl^--$TPeA^+$ exhibited phosphorescence with the λ_{em} at 654, 522 and 509 nm with Φ_{em} (relative intensities to the solid-state **2a**) of 3.6% (5.1), 6.2% (8.9) and 2.6% (3.7), respectively, indicating enhanced phosphorescence properties (Table 4, Fig. 6a, b and S86†). The λ_{em} of **2a**·Cl^--TBA^+ and **2a**·Cl^--$TPeA^+$ were similar to the solution-state λ_{em} of **2a**·Cl^-, suggesting the phosphorescence derived

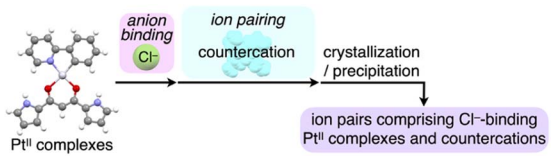

Fig. 5 Preparation procedures of ion-pairing assemblies comprising Cl^--binding Pt^{II} complexes and countercations.

Table 4 Solid-state properties (emission peaks, emission lifetimes and quantum yields) of **2a** and its ion pairs of Cl^- complexes with tetraalkylammonium cations

	λ_{em} [nm]	τ_1 [μs]/ f_1 [%]	τ_2 [μs]/ f_2 [%]	τ_3 [μs]/ f_3 [%]	Φ_{em} [%]
2a	523	140/31	550/69	—	0.7
2a·Cl^--TPA^+	654	110/24	440/76	—	3.6
2a·Cl^--TBA^+	522	2.9/43	23/25	210/32	6.2
2a·Cl^--$TPeA^+$	509	6.3/8	86/24	440/68	2.6

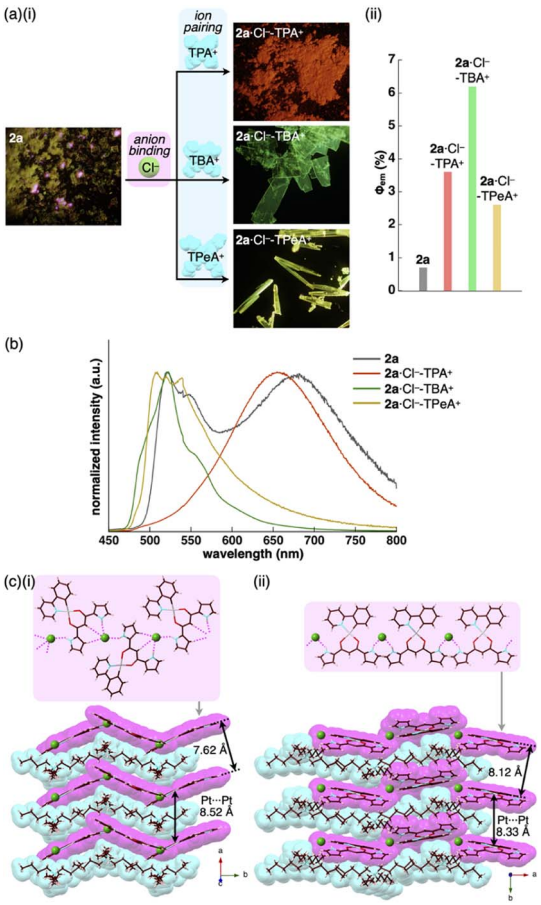

Fig. 6 (a) (i) Photographs and (ii) quantum yields of solid-state **2a**,[13] **2a**·Cl^--TPA^+, **2a**·Cl^--TBA^+ and **2a**·Cl^--$TPeA^+$, (b) solid-state emission spectra of **2a** (grey), **2a**·Cl^--TPA^+ (red), **2a**·Cl^--TBA^+ (green) and **2a**·Cl^--$TPeA^+$ (yellow) and (c) single-crystal X-ray structures of (i) **2a**·Cl^--TBA^+ and (ii) **2a**·Cl^--$TPeA^+$ as top 1D chain and side packing structures. The atom colour code in (c): green (spherical) refers to chlorine. Magenta and cyan denote the receptor–Cl^- complex 1D-chain and cation parts, respectively. For the crystals of **2a** in (a), reflections of excitation light at $UV_{365\ nm}$ were observed in partially pink colour.

from the monomeric Cl^- complex as suggested by single-crystal packing structures (*vide infra*). Notably, **2a**·Cl^--TPA^+ exhibited a distinctive red-shifted emission. The emission lifetimes, such as 440 μs for **2a**·Cl^--$TPeA^+$, were nearly 200 times longer than those of the monomers in solution (Fig. S82†).

The enhanced phosphorescence intensities in the ion-pairing assemblies were investigated using solid-state packing structures revealed by single-crystal X-ray analysis. The ion pair **2a**·Cl^--TBA^+ exhibited an anion-binding mode with hydrogen bonding of the singly inverted pyrrole NH, bridging CH and pyrrole CH (Fig. 6c(i), S24† and Table 5). The Cl^- also interacted with the pyrrole NH of neighbouring **2a**, resulting in a Cl^--bridged 1D-chain structure based on the singly pyrrole-inverted (*py1i*) conformation. Importantly, **2a**·Cl^- and TBA^+ are alternately arranged on the *a*-axis to form a charge-by-charge assembly with a Pt···Pt distance of 8.52 Å. In contrast, crystal-state **2a**·Cl^--$TPeA^+$ exhibited a packing structure with a *py0i* conformation (Fig. 6c(ii) and S25†). The pyrrole NHs of **2a** formed hydrogen bonds independently, resulting in a Cl^--bridged chain structure. **2a**·Cl^- and $TPeA^+$ were alternately arranged to form a charge-by-charge assembly with a Pt···Pt distance of 8.34 Å. The assembling modes, with different numbers of inverted pyrrole rings, are determined by the alkyl chain lengths of the countercations (TBA^+ and $TPeA^+$), resulting in different nearest $Cl^-\cdots Cl^-$ distances of 8.90 and 10.72 Å, respectively. Hirshfeld surface analysis of the crystal structures indicated no characteristic close contacts between the Pt^{II} complex and cation, suggesting that both cations exhibited similar interactions. This is also supported by the energy decomposition analysis (EDA) in the framework of the fragment molecular orbital method at the FMO2-MP2 using mixed basis sets including NOSeC-V-DZP with MCP with TZP for Pt, demonstrating that the dispersion forces were effective between the Pt^{II} complex and cations (Fig. S57 and S58†).[22–25] Although the exact assembling structure for the precipitates of **2a**·Cl^--TPA^+ could not be determined by single-crystal X-ray analysis, synchrotron XRD analysis revealed no characteristic diffraction pattern, suggesting the less ordered arrangement of **2a**·Cl^- and TPA^+ (Fig. S83†). The speculated slipped stacking of **2a**·Cl^- in the solid-state **2a**·Cl^--TPA^+ could be correlated with the red-shifted phosphorescence.

In any ion pairs of **2a**·Cl^-, the isolation of the Pt^{II} complexes by aliphatic cations, required for enhancing phosphorescence intensities, was clearly indicated by the X-ray structures of the ion-pairing assemblies. Furthermore, the rigidification of packing structures by Cl^--bridged 1D-chain structures is vital for enhancing the phosphorescence intensities. The larger Φ_{em} of **2a**·Cl^--TBA^+ than that of **2a**·Cl^--$TPeA^+$ can be ascribed to the stabilization of the 1D-chain structure by hydrogen bonding. The electrostatic energy, revealed by EDA, originating mainly from hydrogen-bonding interactions for the **2a**···Cl^-···**2a** structure in the 1D-chain of **2a**·Cl^--TBA^+ possessed a larger absolute value by 10.7 kcal mol^{-1} than that of **2a**·Cl^--$TPeA^+$ (Fig. S57 and S58†).

Charge-by-charge assemblies were observed in the single-crystal packing structures of **2c,d** with tetraalkylammonium cations (Fig. 7a, S28–S31† and Table 6). A crystal of **2c**·Cl^--TBA^+, prepared from CH_2ClCH_2Cl/*n*-hexane, for example, demonstrated a *py1i* conformation with Cl^- binding by pyrrole NH, β-CH and bridging CH. A Cl^--bridged chain structure similar to **2a**·Cl^--TBA^+ was formed by the interaction between uninverted pyrrole NH and neighbouring Cl^-. In contrast, a single crystal of **2c**·Cl^--$TPeA^+$, prepared from CH_2ClCH_2Cl/*n*-hexane, exhibited a *py0i* conformation and a chain structure (Fig. 7b and S29†) as observed in **2a**·Cl^--$TPeA^+$. Furthermore, crystallization of **2d**·Cl^--TBA^+ from CH_2Cl_2/*n*-hexane (**2d**·Cl^--TBA_M^+) and CH_2ClCH_2Cl/*n*-hexane (**2d**·Cl^--TBA_E^+) produced two pseudo polymorphs, with **2d** exhibiting *py1i* conformations that form Cl^--bridged chain structures in both (Fig. 7c and S31†). In all the ion-pairing assemblies revealed by X-ray analysis, Pt^{II} complexes in Cl^--bridged polymers were isolated by aliphatic cations in charge-by-charge arrangements.

As expected from the crystal packing structures, emission enhancement of the solid-state ion-pairing assemblies of **2c,d** was observed, as was a similar tendency for **2a** (Table 7, Fig. 8a, b, S88 and S89†). For example, solid-state ion pairs **2c**·Cl^--TPA^+,[26] **2c**·Cl^--TBA^+ and **2c**·Cl^--$TPeA^+$ showed the λ_{em} at 507,

Table 5 Summary of the representative distances in the crystal structures of **2a**·Cl^--TBA^+ and **2a**·Cl^--$TPeA^+$

	2a·Cl^--TBA^+	**2a**·Cl^--$TPeA^+$
N(–H)···Cl^- [Å]	3.17, 3.18	3.14
$C_{bridging}$(–H)···Cl^- [Å]	3.78	—
C_β(–H)···Cl^- [Å]	3.63	—
Pt···Pt[a] [Å]	8.52	8.33
$Cl^-\cdots Cl^-$[b] [Å]	8.90	10.72

[a] Distances in charge-by-charge assemblies. [b] Distances in Cl^--bridged 1D-chain structures.

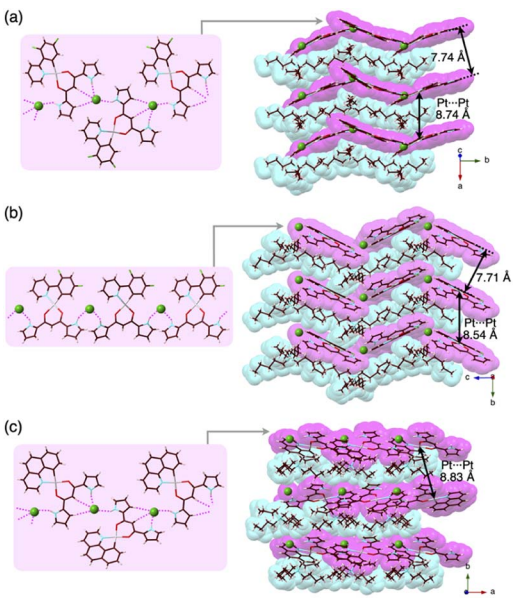

Fig. 7 Single-crystal X-ray structures of (a) **2c**·Cl^--TBA^+, (b) **2c**·Cl^--$TPeA^+$ and (c) **2d**·Cl^--TBA^+_E as top 1D-chain and side packing structures.

Table 6 Summary of the representative distances in the crystal structures of **2c**·Cl^--TBA^+, **2c**·Cl^--$TPeA^+$ and **2d**·Cl^--TBA^+_E

	2c·Cl^--TBA^+	**2c**·Cl^--$TPeA^+$	**2d**·Cl^--TBA_E^+
N(–H)···Cl^- [Å]	3.14, 3.18, 3.19, 3.20	3.14, 3.18	3.10, 3.16
$C_{bridging}$(–H)···Cl^- [Å]	3.84, 3.85	—	3.82
C_β(–H)···Cl^- [Å]	3.65, 3.72	—	3.73
Pt···Pt[a] [Å]	8.74	8.33	8.83
$Cl^-\cdots Cl^-$[b] [Å]	9.01	10.94	8.87

[a] Distances in charge-by-charge assemblies. [b] Distances in Cl^--bridged 1D-chain structures.

Table 7 Solid-state properties (emission peaks, emission lifetimes and quantum yields) of **2c–e** and its ion pairs of Cl^- complexes with tetraalkylammonium cations

	λ_{em} [nm]	τ_1 [μs]/ f_1 [%]	τ_2 [μs]/ f_2 [%]	τ_3 [μs]/ f_3 [%]	Φ_{em} [%]
2c	673	61/90	450/10	—	1.8
2c·Cl^--TPA^+	507	49/15	390/85	—	1.7
2c·Cl^--TBA^+	504	6.3/41	80/14	410/44	3.2
2c·Cl^--$TPeA^+$	515	7.7/10	57/25	390/65	2.4
2d	652	120/28	500/72	—	~0.1[a]
2d·Cl^--TPA^+	627	29/36	190/64	—	1.7
2d·Cl^--TBA^+	563	120/26	490/74	—	0.7
2d·Cl^--$TPeA^+$	594	30/17	330/83	—	0.8
2e	627	100/21	440/79	—	~0.2[a]
2e·Cl^--TPA^+	617	130/28	510/72	—	1.9
2e·Cl^--TBA^+	606	130/27	510/73	—	1.1
2e·Cl^--$TPeA^+$	606	96/18	420/82	—	2.7

[a] Accurate values could not be determined due to low Φ_{em}.

504 and 515 nm with comparable and enhanced Φ_{em} of 1.7%, 3.2% and 2.4%, respectively, due to the formation of charge-by-charge assemblies.[27] Similar to the XRD pattern of **2a**·Cl^--TPA^+, the synchrotron XRD pattern of **2d**·Cl^--TPA^+/$TPeA^+$ precipitates exhibited less clear diffraction patterns with broad peaks, suggesting less ordered arrangements of **2d**·Cl^- and countercations. The Φ_{em} of **2d**·Cl^--TPA^+ was estimated to be 1.7%, which is greater than that of the other **2d**·Cl^- ion pairs. Substituents at π-electronic ligands controlled emissive properties, as observed in the red-shifted phosphorescence at 606–617 nm with enhanced quantum yields of 1.1–2.7% for the ion pairs of **2e**·Cl^- with tetraalkylammonium cations as precipitates (Table 7, Fig. 8c and S90†). Furthermore, the **2b**·Cl^--TPA^+ precipitate obtained from CH_2Cl_2/*n*-hexane exhibited enhanced phosphorescence with a Φ_{em} of 7.5%, which is 75 times greater than that of **2b** (Fig. S87†).[28] The solid-state phosphorescence properties, λ_{em} and Φ_{em}, in ion-pairing assemblies of the anion-responsive Pt^{II} complexes were modulated by the introduced π-electronic C^N ligands and coexisting cations.

Mechanism for phosphorescence enhancement

Enhancing the phosphorescence in the ion-pairing assembly of Pt^{II} complexes was elucidated by DFT calculations based on an ONIOM approach[29,30] for the packing structures of **2a** and **2a**·Cl^--TBA^+. Computational models for solid-state **2a** and **2a**·Cl^--TBA^+ were constructed by cutting out the 1 × 1 × 2 and 3 × 2 × 2 unit cells (Fig. S61 and S67†), where the centre parts and surroundings were treated as quantum mechanics (QM) regions at the DFT level and molecular mechanics (MM) regions at the UFF level, respectively. The electronic structures of the QM region were calculated at the CAM-B3LYP/6-31+G(d,p) and 3-21G with LanL2DZ for Pt in **2a** and **2a**·Cl^--TBA^+, respectively. In both cases, the QM regions exhibited C_i site symmetry.

The optimized S_0 geometry of solid-state **2a** showed pseudo-generate T_1 (A_g) and T_2 (A_u), where A_g and A_u denote the

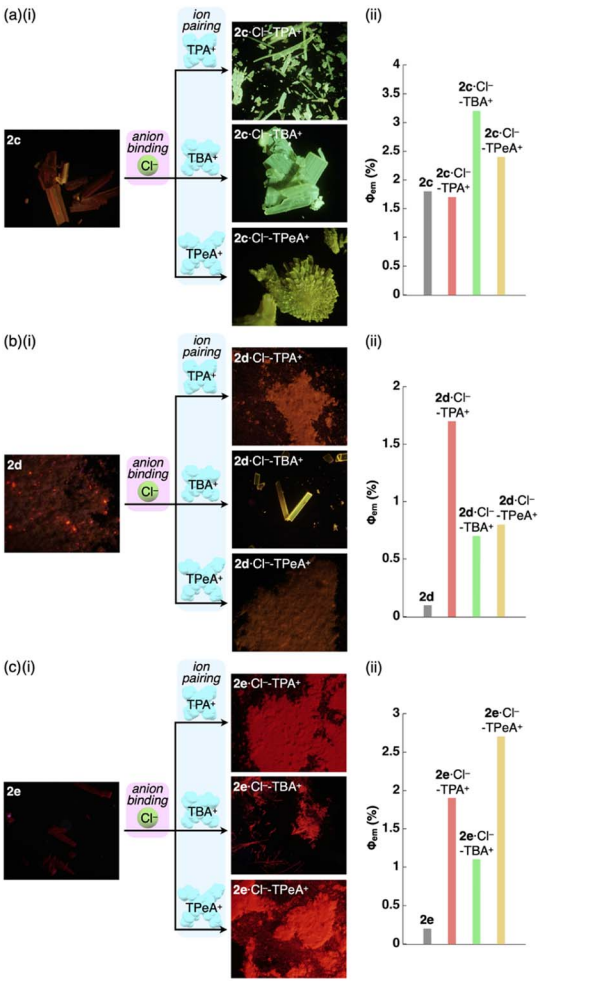

Fig. 8 (i) Photographs and (ii) quantum yields of the Pt^{II} complexes (a) **2c**, (b) **2d** and (c) **2e** and their Cl^- complexes as ion pairs with TPA^+, TBA^+ (**2d**·Cl^--TBA_E^+ for **2d**) and $TPeA^+$ as solid-state samples.

irreducible representations of the excited electronic states, as well as T_3 (A_u) and T_4 (A_g) states, whose wavefunctions were symmetrically delocalized over the **2a** dimer (Fig. S62†). The geometries of T_1 (A_g) and T_4 (A_g) were further optimized owing to the distribution of their wavefunctions at the dipyrrolyldiketone and ppy ligand, respectively. The optimized T_1 and T_4 states with lower symmetries of C_1 owing to a symmetry breaking of pseudo-Jahn–Teller distortion[31] exhibited the lowest excited states with excitation energies of 2.25 eV/551 nm and 1.95 eV/636 nm, respectively (Fig. S63†). The S_0–T_1 electron density difference at the T_1 optimized structure (Fig. 9a(i)) demonstrated that T_1 was an excited state localized on the single molecule. In contrast, the S_0–T_4 electron density difference at the T_4 optimized structure (Fig. 9a(ii)) indicated that T_4 was an excited state with the wavefunction asymmetrically delocalized over the dimer. The calculated phosphorescence spectrum from T_1 reproduced the sharp shape of the experimental spectrum in the short-wavelength region, whereas that from T_4 reproduced the broad shape in the long-wavelength region (Fig. S64†). The T_4 state mainly comprised the HOMO–LUMO transition (the CI coefficient: 0.599) and HOMO-8–LUMO transition (0.234). The HOMO and HOMO-8 originated from the intermolecular interaction between the Pt d_{z^2} orbital in one molecule and the π orbital of the ppy ligand in the other (Fig. 9b).[32] Thus, this intermolecular interaction was responsible for the energetically stable T_4 formation.

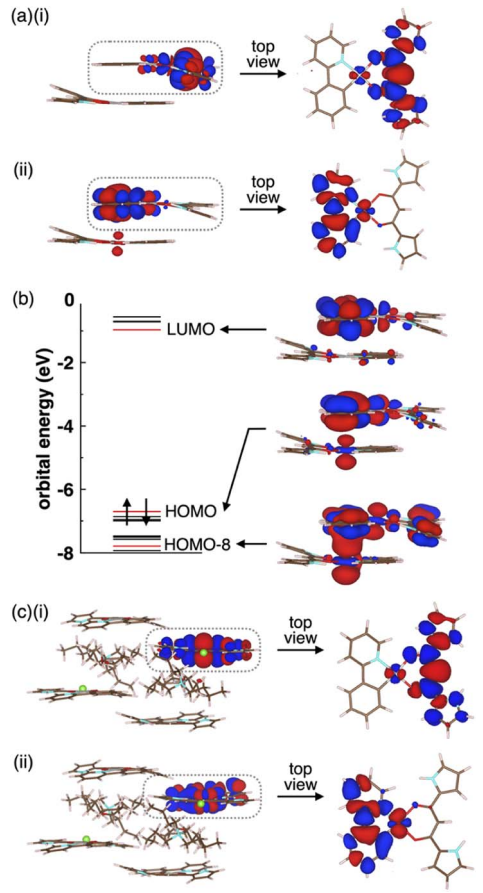

Fig. 9 (a) Electron density differences for solid-state **2a** (i) between S_0 and T_1 at the T_1 optimized structure and (ii) between S_0 and T_4 at the T_4 optimized structure (isosurface value: 5×10^{-4} a.u), (b) orbital levels and molecular orbitals at the T_4 optimized structure (isosurface value: 2×10^{-2} a.u.) and (c) electron density differences for solid-state **2a**·Cl^--TBA^+ (i) between S_0 and T_1 at the T_1 optimized structure and (ii) between S_0 and T_6 at the T_6 optimized structure (isosurface value: 5×10^{-4} a.u.). The red and blue regions are positive and negative in electron density differences, respectively. Only the QM region is shown for simplicity.

The Φ_{em} values depend on nonradiative rate constants from the excited to the ground states. The rate constant significantly increases with diagonal vibronic coupling constants (VCCs) of the final electronic state because of easier acceptance of electronic excitation energy.[33] For the solid-state **2a**, the diagonal VCCs of S_0 at the T_4 optimized structure were larger than those at the T_1-optimized structure (Fig. S65†), suggesting that the nonradiative transition from the T_4 state was fast. Vibronic coupling density (VCD)[33,34] elucidated that the large VCCs arose from the strong coupling between the electronic state and vibrational modes distributed over the ppy ligand (Fig. S66†). Thus, the low Φ_{em} of the solid-state **2a** was attributed to T_4 with large diagonal VCCs.

The charge-by-charge packing structure significantly affected the electronic states of **2a**. In **2a**·Cl^--TBA^+, the pseudo-degenerate T_1 (A_g) and T_2 (A_u) as well as T_3 (A_u) and T_4 (A_g) wavefunctions at the S_0 optimized structure were distributed over the dipyrrolyldiketone unit, whereas the T_5 (A_u) and T_6 (A_g) wavefunctions were distributed over the ppy ligand (Fig. S68†). The optimized geometries of T_1 (A_g) and T_6 (A_g) exhibited the wavefunctions localized on the single molecule by the pseudo-Jahn–Teller distortion (Fig. 9c and S69†). In contrast to the solid-state **2a**, the electronic wavefunction was not delocalized over dimer for these states because of the presence of TBA^+ between **2a**·Cl^-. The TBA^+ in the charge-by-charge assembly clearly decoupled the electronic interaction, resulting in enhanced phosphorescence derived from the monomeric Pt^{II} complex. Although the Φ_{em} values of the ion-pairing assemblies are lower than those in the solution state because of the reduced interactions in the solvated monomeric forms, introduction of aliphatic cations is efficient for inhibiting the self-association and enhancing the phosphorescence properties.

Conclusions

An ion-pairing strategy has been applied for fabricating solid-state phosphorescent materials by isolating dipyrrolyldiketone Pt^{II} complexes, as emissive anion-responsive molecules, in the form of anion complexes with aliphatic cations. Charge compensation between the anion complexes, in anion-bridged rigid chain structures, and countercations interfered with self-association, resulting in enhanced phosphorescence emission. Solid-state arrangement of the Pt^{II} complexes and their photophysical properties were influenced by the introduced arylpyridine ligands and coexisting cations. Furthermore, the facile recrystallization procedures in the ion-pairing strategy for preparing luminescent materials can be applied for large-scale production. The ion-pairing strategy used in this study does not require the solution-state anion-binding mode. To the best

of our knowledge, such a room-temperature phosphorescence enhancement by anion binding and ion-pairing assembly has not been demonstrated thus far. The mechanism of the phosphorescence intensity modulated by anion binding and ion pairing was clearly revealed by theoretical studies for stacking structures. Assembly systems with multiple components, based on the combination of host systems and cationic species, would provide diverse materials with controllable emission wavelengths, quantum yields and lifetimes. Introducing more bulky and robust countercations would further improve the solid-state emission properties. Moreover, introduction of π-electronic cations[35] would also result in the formation of materials with intriguing photophysical properties. Further studies on ion-pairing luminescent materials are currently being conducted by designing and synthesizing charged building units and precursors (ion-responsive molecules).

Data availability

Data supporting the work in this publication are available *via* the ESI and associated crystallographic data.†

Author contributions

H. M. designed and conducted the project. Y. H., K. K., Y. M. and H. T. carried out the synthesis, characterization and property examinations. H. S., H. I. and N. T. evaluated the solid-state absorption and emission spectra. W. O. and T. S. conducted the theoretical calculations. Y. H. and N. Y. analyzed the single-crystal X-ray structures.

Conflicts of interest

There are no conflicts of interest to declare.

Acknowledgements

This work was supported by JSPS KAKENHI Grant Numbers JP18H01968 and JP22H02067 for Scientific Research (B), JP19K05444 and JP22K05253 for Scientific Research (C), JP20J22745 for JSPS Fellows and JP20H05863 for Transformative Research Areas (A) "Condensed Conjugation" and the Ritsumeikan Global Innovation Research Organization (R-GIRO) project (2017–22 and 2022–27). Theoretical calculations were partially performed using the Research Center for Computational Science, Okazaki, Japan (Projects: 19-IMS-C085, 20-IMS-C079, 21-IMS-C077 and 22-IMS-C077) and Information Initiative Center, Hokkaido University. The synchrotron radiation experiments were performed at BL02B1 (2019B1638), BL40XU (2021B1703) and BL40B2 (2021B1828) with the approval of the Japan Synchrotron Radiation Research Institute (JASRI). We thank Prof. Atsuhiro Osuka, Dr Takayuki Tanaka, Dr Akito Nakai and Dr Koki Kise, Kyoto University, for single-crystal X-ray analysis, Dr Kunihisa Sugimoto, Kindai University, for synchrotron radiation single-crystal X-ray analysis, Dr Noboru Ohta, JASRI/SPring-8, for synchrotron radiation XRD analysis, Prof. Shigeki Kuwata, Ritsumeikan University, for elemental analysis and Prof. Hitoshi Tamiaki, Ritsumeikan University, for various measurements.

Notes and references

1 Selected books and reviews on supramolecular assemblies for electronic materials: (*a*) *Functional Supramolecular Architectures: For Organic Electronics and Nanotechnology*, ed. P. Samorì and F. Cacialli, Wiley, 2011; (*b*) *Supramolecular Materials for Opto-Electronics*, ed. N. Koch, RSC, 2015; (*c*) T. Wöhrle, I. Wurzbach, J. Kirres, A. Kostidou, N. Kapernaum, J. Litterscheidt, J. C. Haenle, P. Staffeld, A. Baro, F. Giesselmann and S. Laschat, *Chem. Rev.*, 2016, **116**, 1139–1241; (*d*) P. Yu, Y. Zhen, H. Dong and W. Hu, *Chem*, 2019, **5**, 2814–2853; (*e*) C. J. Kousseff, R. Halaksa, Z. S. Parr and C. B. Nielsen, *Chem. Rev.*, 2022, **122**, 4397–4419; (*f*) J. Chen, W. Zhang, L. Wang and G. Yu, *Adv. Mater.*, 2023, **35**, 2210772.

2 J. Gierschner, J. Shi, B. Milián-Medina, D. Roca-Sanjuán, S. Varghese and S. Y. Park, *Adv. Opt. Mater.*, 2021, **9**, 2002251.

3 (*a*) V. W.-W. Yam, V. K.-M. Au and S. Y.-L. Leung, *Chem. Rev.*, 2015, **115**, 7589–7728; (*b*) T. Strassner, *Acc. Chem. Res.*, 2016, **49**, 2680–2689; (*c*) L. Ravotto and P. Ceroni, *Coord. Chem. Rev.*, 2017, **346**, 62–76; (*d*) E. V. Puttock, M. T. Walden and J. A. G. Williams, *Coord. Chem. Rev.*, 2018, **367**, 127–162; (*e*) M. Yoshida and M. Kato, *Coord. Chem. Rev.*, 2020, **408**, 213194; (*f*) Y. Han, Z. Gao, C. Wang, R. Zhong and F. Wang, *Coord. Chem. Rev.*, 2020, **414**, 213300.

4 (*a*) V. W.-W. Yam, K. M.-C. Wong and N. Zhu, *J. Am. Chem. Soc.*, 2002, **124**, 6506–6507; (*b*) Y. Sun, K. Ye, H. Zhang, J. Zhang, L. Zhao, B. Li, G. Yang, B. Yang, Y. Wang, S.-W. Lai and C.-M. Che, *Angew. Chem., Int. Ed.*, 2006, **45**, 5610–5613; (*c*) N. Komiya, M. Okada, K. Fukumoto, D. Jomori and T. Naota, *J. Am. Chem. Soc.*, 2011, **133**, 6493–6496; (*d*) C.-H. Chen, F.-I. Wu, Y.-Y. Tsai and C.-H. Cheng, *Adv. Funct. Mater.*, 2011, **21**, 3150–3158; (*e*) N. Komiya, N. Itami and T. Naota, *Chem. – Eur. J.*, 2013, **19**, 9497–9505; (*f*) M. Mauro, A. Aliprandi, C. Cebrián, D. Wang, C. Kübel and L. De Cola, *Chem. Commun.*, 2014, **50**, 7269–7272; (*g*) K. Ohno, S. Yamaguchi, A. Nagasawa and T. Fujihara, *Dalton Trans.*, 2016, **45**, 5492–5503; (*h*) M.-J. Sun, Y. Liu, W. Zeng, Y. S. Zhao, Y.-W. Zhong and J. Yao, *J. Am. Chem. Soc.*, 2019, **141**, 6157–6161; (*i*) H. Yang, H. Li, L. Yue, X. Chen, D. Song, X. Yang, Y. Sun, G. Zhou and Z. Wu, *J. Mater. Chem. C*, 2021, **9**, 2334–2349; (*j*) F.-F. Xu, W. Zeng, M.-J. Sun, Z.-L. Gong, Z.-Q. Li, Y. S. Zhao, J. Yao and Y.-W. Zhong, *Angew. Chem., Int. Ed.*, 2022, **61**, e202116603.

5 M. Kasha, H. R. Rawls and M. Ashraf El-Bayoumi, *Pure Appl. Chem.*, 1965, **11**, 371–392.

6 D. L. Dexter and J. H. Schulman, *J. Chem. Phys.*, 1954, **22**, 1063–1070.

7 Pt···Pt interaction is another factor to enhance emissions for the Pt^{II} complexes that have appropriate electronic structures, although resulting metal-metal-to-ligand charge transfer (MMLCT) gives rise to the photophysical properties differing from those of monomeric states. See also ref. 4*h*.

8 (*a*) Z. Cheng, H. Shi, H. Ma, L. Bian, Q. Wu, L. Gu, S. Cai, X. Wang, W.-w. Xiong, Z. An and W. Huang, *Angew. Chem., Int. Ed.*, 2018, **57**, 678–682; (*b*) S. Cai, H. Ma, H. Shi, H. Wang, X. Wang, L. Xiao, W. Ye, K. Huang, X. Cao, N. Gan, C. Ma, M. Gu, L. Song, H. Xu, Y. Tao, C. Zhang, W. Yao, Z. An and W. Huang, *Nat. Commun.*, 2019, **10**, 4247.

9 (*a*) C. F. J. Faul, *Acc. Chem. Res.*, 2014, **47**, 3428–3438; (*b*) K. Goossens, K. Lava, C. W. Bielawski and K. Binnemans, *Chem. Rev.*, 2016, **116**, 4643–4807.

10 Reviews and the first report by our group: (*a*) Y. Haketa, K. Urakawa and H. Maeda, *Mol. Syst. Des. Eng.*, 2020, **5**, 757–771; (*b*) Y. Haketa, K. Yamasumi and H. Maeda, *Chem. Soc. Rev.*, 2023, **52**, 7170–7198; (*c*) Y. Haketa, S. Sasaki, N. Ohta, H. Masunaga, H. Ogawa, N. Mizuno, F. Araoka, H. Takezoe and H. Maeda, *Angew. Chem., Int. Ed.*, 2010, **49**, 10079–10083.

11 (*a*) Z.-m. Ou, H. Yao and K. Kimura, *J. Photochem. Photobiol., A*, 2007, **189**, 7–14; (*b*) D. K. Bwambok, B. El-Zahab, S. K. Challa, M. Li, L. Chandler, G. A. Baker and I. M. Warner, *ACS Nano*, 2009, **4**, 3854–3860; (*c*) Y. Yang, C. Sun, S. Wang, K. Yan, M. Zhao, B. Wu and F. Zhang, *Angew. Chem., Int. Ed.*, 2022, **61**, e202117436.

12 (*a*) C. R. Benson, L. Kacenauskaite, K. L. VanDenburgh, W. Zhao, B. Qiao, T. Sadhukhan, M. Pink, J. Chen, S. Borgi, C.-H. Chen, B. J. Davis, Y. C. Simon, K. Raghavachari, B. W. Laursen and A. H. Flood, *Chem*, 2020, **6**, 1978–1997; (*b*) L. Kacenauskaite, S. G. Stenspil, A. H. Olsson, A. H. Flood and B. W. Laursen, *J. Am. Chem. Soc.*, 2022, **144**, 19981–19989.

13 A. Kuno, G. Hirata, H. Tanaka, Y. Kobayashi, N. Yasuda and H. Maeda, *Chem. – Eur. J.*, 2021, **27**, 10068–10076.

14 Negatively charged luminescent species can be obtained by anion binding by electronically neutrally charged π-electronic systems. Actually, since the first report on π-electronic ion-pairing assemblies based on dipyrrolyldiketone boron complexes as anion-responsive π-electronic systems (ref. 10*c*), new properties and functions derived from the ordered arrangement of charged π-systems have been revealed (ref. 10*a* and *b*). Replacement of boron with other metal ions would induce new π-electronic systems and ion-pairing assemblies. However, dipyrrolyldiketones form complexes, comprising a single diketone unit, with only Pt^{II} in a square planar fashion (ref. 13).

15 Z. M. Hudson, B. A. Blight and S. Wang, *Org. Lett.*, 2012, **14**, 1700–1703.

16 M. J. Frisch, *et al.*, *Gaussian 09, Revision D.01*, Gaussian, Inc., Wallingford CT, 2013.

17 (*a*) J. Brooks, Y. Babayan, S. Lamansky, P. I. Djurovich, I. Tsyba, R. Bau and M. E. Thompson, *Inorg. Chem.*, 2002, **41**, 3055–3066; (*b*) D. Wang, X. Chen, H. Yang, D. Zhong, B. Liu, X. Yang, L. Yue, G. Zhou, M. Ma and Z. Wu, *Dalton Trans.*, 2020, **49**, 15633–15645; (*c*) A. Haque, H. E. Moll, K. M. Alenezi, M. S. Khan and W.-Y. Wong, *Materials*, 2021, **14**, 4236.

18 The photophysical properties were examined for the single crystals, lightly crushed with a spatula, on a quartz plate. The crystals showed no significant changes in the XRD patterns.

19 (*a*) B. Ma, P. I. Djurovich and M. E. Thompson, *Coord. Chem. Rev.*, 2005, **249**, 1501–1510; (*b*) T. Shigehiro, S. Yagi, T. Maeda, H. Nakazumi, H. Fujiwara and Y. Sakurai, *J. Phys. Chem. C*, 2013, **117**, 532–542; (*c*) Y.-J. Cho, S.-Y. Kim, H.-J. Son, D. W. Cho and S. O. Kang, *Phys. Chem. Chem. Phys.*, 2017, **19**, 5486–5494.

20 P. R. Spackman, M. J. Turner, J. J. McKinnon, S. K. Wolff, D. J. Grimwood, D. Jayatilaka and M. A. Spackman, *J. Appl. Crystallogr.*, 2021, **54**, 1006–1011.

21 Crystal polymorphs were observed for **2a** in the photograph, and the details will be discussed elsewhere.

22 Articles for *GAMESS*: (*a*) M. W. Schmidt, K. K. Baldridge, J. A. Boatz, S. T. Elbert, M. S. Gordon, J. H. Jensen, S. Koseki, N. Matsunaga, K. A. Nguyen, S. Su, T. L. Windus, M. Dupuis and J. A. Montgomery Jr, *J. Comput. Chem.*, 1993, **14**, 1347–1363; (*b*) M. S. Gordon, and M. W. Schmidt, in *Theory and Applications of Computational Chemistry: The First Forty Years*, ed. C. E. Dykstra, G. Frenking, K. S. Kim and G. E. Scuseria, Elsevier, 2005.

23 M. J. S. Phipps, T. Fox, C. S. Tautermann and C.-K. Skylaris, *Chem. Soc. Rev.*, 2015, **44**, 3177–3211.

24 Report for FMO: K. Kitaura, E. Ikeo, T. Asada, T. Nakano and M. Uebayasi, *Chem. Phys. Lett.*, 1999, **313**, 701–706.

25 Report for pair interaction energy decomposition analysis (PIEDA): D. G. Fedorov and K. Kitaura, *J. Comput. Chem.*, 2007, **28**, 222–237.

26 The preliminarily examined single-crystal X-ray analysis of **2c**·Cl^--TPA^+ for the crystal of low quality revealed the formation of a charge-by-charge assembly.

27 The electrostatic energy, revealed by EDA, originating mainly from hydrogen-bonding interactions for the **2c**···Cl^-···**2c** structure in the 1D chain of **2c**·Cl^--TBA^+ was larger in the absolute value by 13.5 kcal/mol than that of **2c**·Cl^--$TPeA^+$, resulting in a larger Φ_{em} for **2c**·Cl^--TBA^+.

28 **2b** and TPACl were included in **2b**·Cl^--TPA^+ in a 1:1 ratio as determined by ^{1}H NMR. Notably, **2b**, in the *py1i* conformation, formed a [4 + 1]-type anion complex $\mathbf{2b}_4$·Cl^- as ion pairs with TBA^+ and $TPeA^+$ (Fig. S26 and 27†). Their solid-state emission properties would be discussed elsewhere owing to the difficulty of preparing crystals.

29 M. J. Frisch, *et al.*, *Gaussian 16, Revision C.01*, Gaussian, Inc., Wallingford CT, 2016.

30 L. W. Chung, W. M. C. Sameera, R. Ramozzi, A. J. Page, M. Hatanaka, G. P. Petrova, T. V. Harris, X. Li, Z. Ke, F. Liu, H.-B. Li, L. Ding and K. Morokuma, *Chem. Rev.*, 2015, **115**, 5678–5796.

31 I. B. Bersuker and V. Z. Polinger, *Vibronic Interactions in Molecules and Crystals*, Springer, 1989.

32 (*a*) D. Kim and J.-L. Brédas, *J. Am. Chem. Soc.*, 2009, **131**, 11371–11380; (*b*) W.-C. Chen, C. Sukpattanacharoen, W.-H. Chan, C.-C. Huang, H.-F. Hsu, D. Shen, W.-Y. Hung, N. Kungwan, D. Escudero, C.-S. Lee and Y. Chi, *Adv. Funct. Mater.*, 2020, **30**, 2002494; (*c*) P. Pander, A. Sil, R. J. Salthouse, C. W. Harris, M. T. Walden, D. S. Yufit,

J. A. G. Williams and F. B. Dias, *J. Mater. Chem. C*, 2022, **10**, 15084–15095.

33 (*a*) M. Uejima, T. Sato, D. Yokoyama, K. Tanaka and J.-W. Park, *Phys. Chem. Chem. Phys.*, 2014, **16**, 14244–14256; (*b*) W. Ota, M. Uejima and T. Sato, *Bull. Chem. Soc. Jpn.*, 2023, **96**, 582–590.

34 (*a*) T. Sato, K. Tokunaga and K. Tanaka, *J. Phys. Chem. A*, 2008, **112**, 758–767; (*b*) T. Kato, N. Haruta and T. Sato, *Vibronic Coupling Density: Understanding Molecular Deformation*, Springer, 2021.

35 (*a*) [2 + 1]-type complex $\mathbf{2d}_2 \cdot Cl^-$ formed an ion pair with tetraphenylporphyrin Au^{III} complex as a π-electronic cation (Fig. S32†); (*b*) Y. Haketa, Y. Bando, Y. Sasano, H. Tanaka, N. Yasuda, I. Hisaki and H. Maeda, *iScience*, 2019, **14**, 241–256; (*c*) H. Tanaka, Y. Kobayashi, K. Furukawa, Y. Okayasu, S. Akine, N. Yasuda and H. Maeda, *J. Am. Chem. Soc.*, 2022, **144**, 21710–21718.